Available online at www.sciencedirect.com
SCIENCE DIRECT
Catalysis Today 113 (2006) 16–24
CATALYSIS TODAY
www.elsevier.com/locate/cattod

Simultaneous operando EPR/UV–vis/laser–Raman spectroscopy — A powerful tool for monitoring transition metal oxide catalysts during reaction

Angelika Brückner *, Evgueni Kondratenko

Institut für Angewandte Chemie Berlin-Adlershof e. V., Richard-Willstätter-Str. 12, D-12489 Berlin, Germany

Available online 4 January 2006

Abstract

This paper represents the extended version of a short communication [Chem. Commun. (2005) 1761] in which for the first time, a setup is presented by which operando EPR, UV–vis and laser–Raman spectra as well as catalytic activity and selectivity can be recorded simultaneously during heterogeneous catalytic gas-phase reactions from the same solid catalyst under identical reaction conditions. In comparison to the separate single-technique applications, this novel triple coupling provides more comprehensive and more relevant information about the working catalytic system since problems arising from differences in reaction conditions and cell designs are avoided and a broader range of catalyst properties can be assessed. The technique has been used to study structure–function relationships in a supported V/TiO_2 catalyst during oxidative dehydrogenation of propane. Benefits arising in comparison to single-technique approaches are discussed.

Keywords: Operando EPR/UV–vis/Raman spectroscopy; V/TiO_2 catalysts; Oxidative dehydrogenation of propane

1. Introduction

A recent trend of growing importance in catalysis research comprises monitoring of catalysts *in status operandi* with simultaneous analysis of product composition by more than one physico-chemical technique at the same time and in the same reactor. For this type of experiments, the label ''operando spectroscopy'' has been introduced a few years ago [1–3]. Besides time saving being certainly not the crucial advantage, such couplings might lead to more comprehensive and more relevant results since problems arising from differences in reaction conditions and cell designs are avoided and a broader range of catalyst properties can be assessed. After introduction of the first simultaneous coupling of two operando methods, namely XRD/QEXAFS/on line MS [4,5], simultaneous EPR/UV–vis–DRS/on line-GC was the second example of parallel operando studies [6]. It has been shown that special benefits can be derived by the latter coupling, in particular, for operando studies of transition metal oxide catalysts, e.g. of supported VO_x and CrO_x catalysts in oxidative and non-oxidative dehydrogenation of propane, due to the fact that EPR and UV–vis–DRS are to a certain extent complementary techniques. While EPR detects sensitively paramagnetic transition metal ions (TMI) such as V^{4+}, Cr^{5+} and Cr^{3+}, UV–vis–DRS is a powerful monitor for diamagnetic TMI such as V^{5+} and Cr^{6+}, since the latter give rise to intense charge-transfer (CT) transitions. Parallel operando UV–vis/Raman studies of a supported Cr/Al_2O_3 catalyst illustrated impressively the benefits that can be gained by this combination for monitoring different states of the active metal oxide phase as well as deactivation/regeneration processes in propane dehydrogenation [7]. Other recently established couplings of operando techniques comprise UV–vis/XAFS [8], MAS-NMR/UV–vis [9] and thermal analysis/FT-IR spectroscopy [10].

In this work, we present a more comprehensive description of results that have been obtained for the first time by coupling three operando techniques, namely EPR, UV–vis–DRS and laser–Raman spectroscopy for monitoring the oxidative dehydrogenation of propane over vanadia supported on TiO_2 [11]. Besides operando EPR and UV–vis–DRS, the potential of

* Corresponding author at: Institut für Angewandte Chemie Berlin-Adlershof e. V., P.O. Box 96 11 56, D-12474 Berlin, Germany. Tel.: +49 30 6392 4301; fax: +49 30 6392 4454.
E-mail address: brueckner@aca-berlin.de (A. Brückner).

0920-5861/$ – see front matter
doi:10.1016/j.cattod.2005.11.006

which for monitoring vanadia-based catalysts in different reactions has been illustrated in a number of papers [12–17], laser–Raman spectroscopy alone has been extensively used in the past for elucidating the structure and behaviour of VO_x species dispersed on a multitude of different oxide supports during oxidative and reductive thermal treatment [18,19] as well as during oxidation of hydrocarbons such as methanol [20], *n*-butane [21,22], methane [23], ethane [24] and propane [16,25].

By using the three techniques in parallel, comprehensive information on the structure and behaviour of different V sites in the catalyst is available. Thus, operando EPR spectroscopy is sensitive for tetravalent vanadium sites in distorted octahedral and/or square–pyramidal geometry either as isolated VO^{2+} species or as interacting VO^{2+} sites within oxidic V_xO_y clusters, while V^{4+} in distorted tetrahedral symmetry is usually not detected at temperatures above −196 °C due to short relaxation times. In contrast, UV–vis spectroscopy is rather suitable for the analysis of pentavalent V sites since intense charge-transfer (CT) transitions are observed in the spectra while reduced V species (V^{4+} and/or V^{3+}) are difficult to distinguish since bands of the respective d–d transitions are usually very broad and weak. Raman spectroscopy, on the other hand, is sensitive for metal–oxygen vibrations. In the case of VO_x species, bands fall into three different regions which have been generally assigned to terminal V^{5+}=O groups of isolated and/or polymeric one- or two-dimensional V_xO_y surface species (1000–1040 cm^{-1}) and V_2O_5 nanocrystallites (≈995 cm^{-1}) and to V^{5+}–O–V^{5+} vibrations of polymeric V_xO_y surface species (750–950 cm^{-1}). In VO_x/TiO_2 catalysts, those bands were observed at ≈1030, 997 and 920–950 cm^{-1}, respectively [18,20]. Vibrations of reduced $V^{4+/3+}$–O moieties are rarely observed [18]. It has been claimed that this might be due to the absence of V=O bonds in reduced VO_x species [19,20] although, at least for VO^{2+}, this is not true. Moreover, there exist different opinions on the structure of isolated VO_x sites on TiO_2. While Burcham et al. [20] regard those species as being tetrahedral on all supports, Went et al. [18] discussed square–pyramidal O=VO_4 moieties on the surface of anatase. Also, there are some doubts whether the observed shift and intensity loss of the Raman bands of VO_x/TiO_2 during methanol oxidation at low temperature are due to reduction of V^{5+} or rather to the coordination of methoxy species to these sites [20].

In this paper, the improvement of information will be illustrated that can be gained by simultaneously coupling operando EPR, UV–vis and laser–Raman spectroscopy in relation to the separate use of these techniques.

2. Experimental

The experimental setup for parallel operando EPR/UV–vis/Raman studies is shown in Fig. 1. A fixed-bed tubular quartz reactor with an inner diameter of 3 mm located within a double-wall quartz dewar is placed into the rectangular cavity of an ELEXSYS 500-10/12 c.w. spectrometer (Bruker). Heat is transferred to the sample by a pre-heated stream of nitrogen. The flow rate and the heater power are controlled by a Bruker variable temperature control unit. EPR spectra in X-band ($\nu \approx 9.5$ GHz) were recorded using a microwave power of 6.3 mW, a modulation frequency of 100 kHz, and a modulation

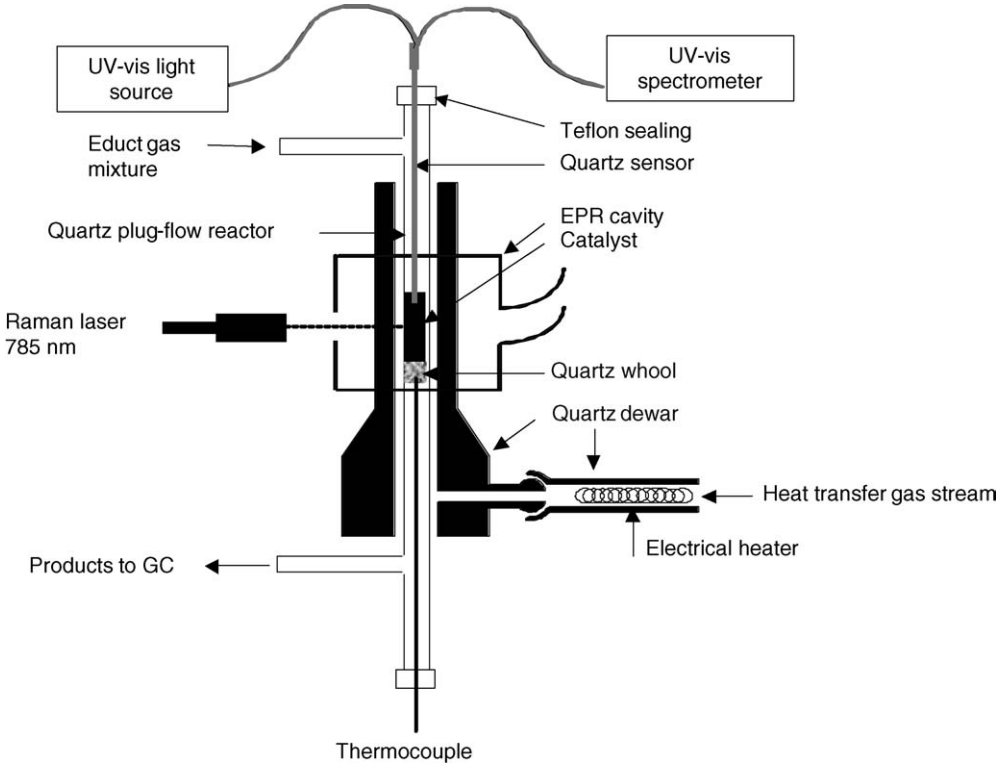

Fig. 1. Experimental setup for parallel operando EPR/UV–vis/Raman measurements.

amplitude of 0.5 mT. The magnetic field was measured with reference to the standard 2,2-diphenyl-1-picrylhydracyl hydrate (DPPH). Computer simulation of V^{4+} EPR spectra was performed with the program SIM14S of Lozos et al. [26] using the spin Hamiltonian:

$$H = \mu_B S B_0 + \mathrm{SAI} \quad (1)$$

in which μ_B is the Bohr magneton, S, the electron spin operator, g, the g tensor, B_0, the magnetic field vector, A, the hyperfine tensor and I is the nuclear spin operator.

For simultaneous recording of UV–vis reflectance spectra, an AVASPEC fibre optical spectrometer (Avantes) equipped with a DH-2000 deuterium–halogen light source and a CCD array detector was used. A cylindrical quartz sensor (Optran UV 1500/1800 T, length 200 mm, diameter 1.5 mm, CeramOptec GmbH) fits into the reactor through a Teflon sealing disk, which is fixed by a screwing at the top end of the reaction tube. The tip of the sensor is a plane-polished surface. It is placed within the catalyst bed. The sensor is connected to the spectrometer and the light source by fibre optical cables (length 2 m) consisting of a core of pure silica (diameter 0.4 mm) coated with polyimide. The feed-through of the thermocouple at the bottom end of the reaction tube is realized in the same way as described for the UV–vis sensor.

Raman spectra were simultaneously recorded by a Raman RXN fibre optical spectrometer (Kaiser Optical Systems). The beam of a 785 nm diode laser was focused on the catalyst bed through a hole in the front side of the EPR cavity. Raman spectra were recorded with a laser power of 25 mW and an acquisition time of 3 s. Five scans were accumulated for each spectrum. The reactant gas flow was mixed by a gas dosing system containing mass flow controllers (Bronckhorst). For on-line product analysis, the reactor outlet was connected to a GC 17AAF capillary gas chromatograph (Shimadzu) equipped with a FID and a 30 m × 0.32 mm Silicaplot column (Chrompack).

Prior to the operando experiments, the catalyst particles (60 mg, 250–355 μm) were heated in a flow of air (10 ml/min) up to 450 °C, held at this temperature for 30 min and cooled to room temperature in the same flow to remove adsorbed moisture and to reoxidize partially reduced vanadium sites. Operando experiments were performed after two different procedures: (a) stepwise heating of the catalyst with 10 K/min in a mixture of 8.3% C_3H_8, 8.3% O_2/N_2 (total flow: 24 ml/min) to different temperatures with 10 min isothermal hold at each temperature for recording the spectra and GC analyses and (b) 20 min isothermal treatment at 300 °C using different ratios of O_2 and C_3H_8 in the feed (O_2/C_3H_8 = 2:1, 1:1 and 1:2, balance: 20 ml N_2, total flow: 24 ml/min). This means, that the time difference between subsequent spectra was 15–20 min in these experiments. However, it should be noted that the intrinsic time resolution of the three spectroscopic methods is markedly higher. In principle, an EPR spectrum comprising a field range of 2000 G can be recorded within 5 min, while depending on the number of scans needed to obtain high signal-to-noise ratios, the time resolution of the Raman spectra can be in the order of seconds. The highest time resolution, being in the order of ms is provided by the UV–vis spectrometer.

Simultaneous TPR/UV–vis measurements were performed in a quartz tube reactor with 100 mg of catalyst. Prior to the TPR analysis, the sample was heated with 10 °C/min to 600 °C in a flow of air (40 ml/min), held at this temperature for 0.5 h and cooled to 25 °C in the same flow. After this oxidising pre-treatment the catalyst was flushed at 25 °C with Ne, heated in a flow of 5% H_2/N_2 (flow rate of 40 ml/min) with 15 °C/min up to 700 °C and held at this temperature for 1 h. Hydrogen consumption and water formation were monitored using a quadruple mass spectrometer (Balzer Omnistar). The following

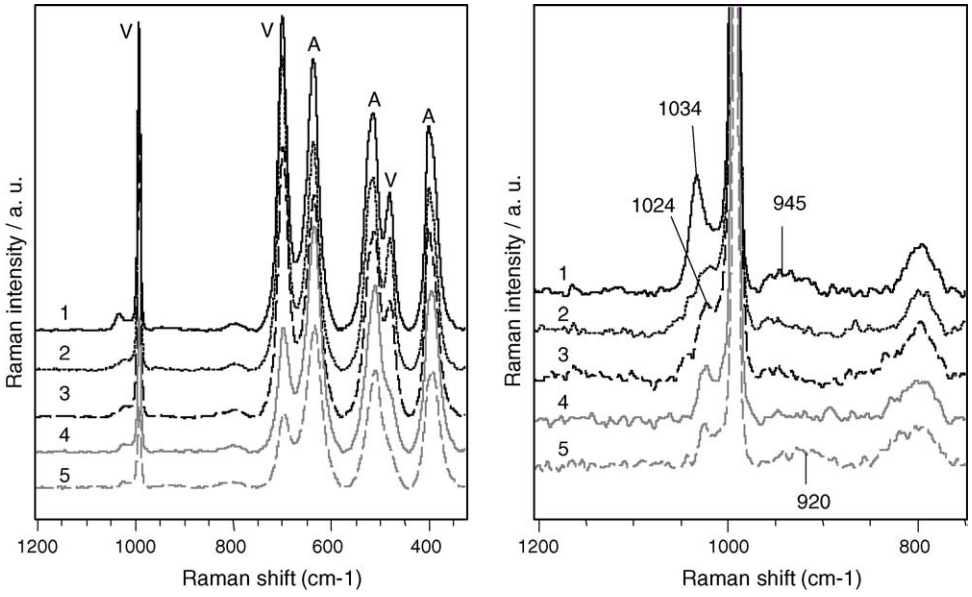

Fig. 2. Raman spectra: (1) at 20 °C after 30 min pre-treatment at 450 °C in air flow and during subsequent heating in a flow of 8.3% O_2, 8.3% C_3H_8/N_2 (24 ml/min), each spectrum recorded after 10 min at 20 °C (2), 100 °C (3), 150 °C (3) and 200 °C (4). Bands of crystalline V_2O_5 and anatase are labelled with V and A, respectively. Right side shows an enlarged section of spectra on left side.

atomic mass units (AMUs) were analyzed: 28 (N_2), 18 (H_2O) and 2 (H_2). For simultaneous UV–vis measurements, a similar AVASPEC fibre optical spectrometer and connecting cables as for EPR/UV–vis/Raman studies were used. A high-temperature reflection probe consisting of six radiating and one reading optical fibre was located inside the reactor furnace perpendicular to the reactor tube (similar to the Raman laser in Fig. 1).

A 6 wt.% V/TiO_2 catalyst was used which was prepared by thermal spreading of V_2O_5 on a commercial anatase carrier (80 m^2/g, 2.2% sulfate, Millennium Chemicals). The appropriate amount of V_2O_5 was mixed with the support by intense grinding in an achate mortar followed by calcination in air flow at 600 °C.

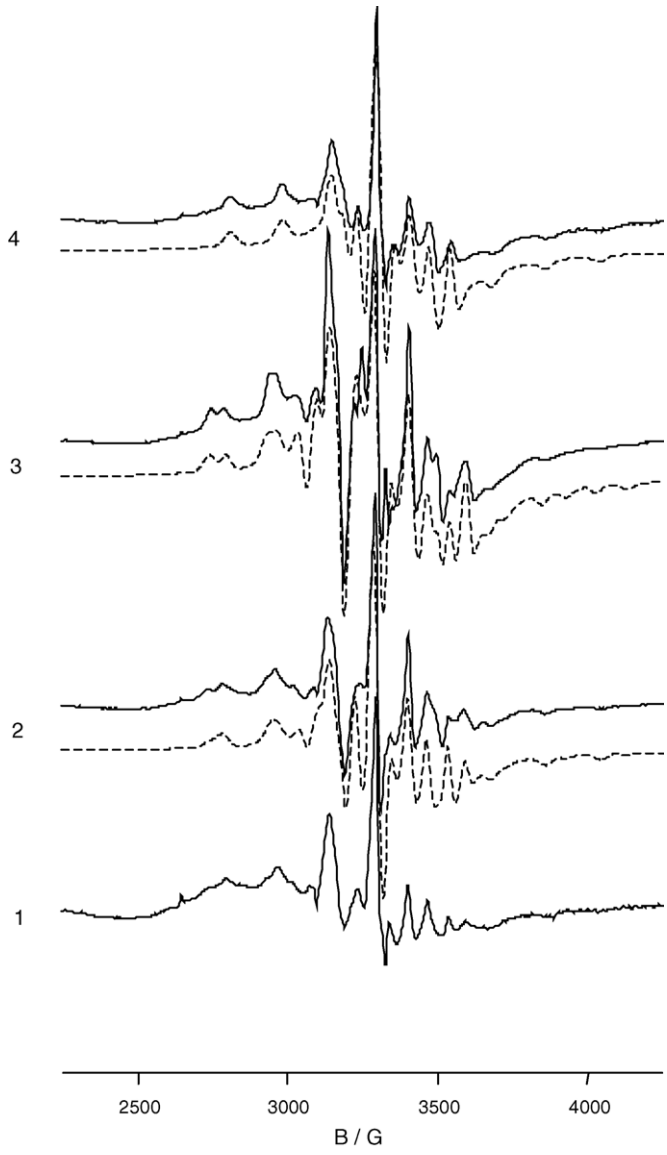

Fig. 3. . EPR spectra recorded in parallel to the Raman spectra in Fig. 2: at 20 °C after pre-treatment at 450 °C in air flow (a), at 20 °C after subsequent 30 min treatment in a flow of 8.3% O_2, 8.3% C_3H_8/N_2 (24 ml/min) (b), at 250 °C after 10 min treatment in the same flow (c) and at 20 °C under feed flow at the end of the experiment (d). Spectra calculated after Eq. (1) are shown as dashed lines.

3. Results and discussion

3.1. Room temperature spectra after oxidative pre-treatment

The room temperature Raman spectrum of the oxidatively pre-treated catalyst (30 min in air flow at 450 °C) shows, besides bands of the anatase carrier marked by A, some bands of crystalline V_2O_5 at 995, 701 and 481 cm^{-1} marked with V (Fig. 2). Additionally, a band at 1034 cm^{-1} with a shoulder extending to lower wave numbers is observed which is assigned to V=O vibrations of VO_x surface species (Fig. 2, right side) [18,19]. The band around 950 cm^{-1} arising from V–O–V vibrations of polymeric V_xO_y surface species [18,19] is only very weak and broad. The band around 800 cm^{-1} is due to the support.

The corresponding room temperature EPR spectrum after oxidative pre-treatment shows a weak signal with poorly resolved hyperfine structure due to coupling of the electron spin ($S = 1/2$) with the nuclear spin of vanadium ($I = 7/2$) (Fig. 3, spectrum 1). Since this signal persists oxidative pre-treatment at 450 °C, it arises probably from VO^{2+} species, which are not accessible by gaseous oxygen due to inclusion within the support matrix and/or the V_2O_5 crystallites.

The respective room temperature UV–vis spectrum shows a broad band around 470 nm being characteristic of a CT transition of V_2O_5 microcrystals [27] (Fig. 4). Unfortunately, CT bands of isolated and low polymerized VO_x species that fall below 400 nm [27], are obscured by the strong absorption of TiO_2.

3.2. Effect of feed treatment at room temperature

Upon switching from air to a flow of 8.3% C_3H_8, 9% O_2/N_2 at room temperature, the Raman signals of V_2O_5 microcrystals and of anatase remain unchanged, but the band at 1034 cm^{-1} diminishes immediately leaving behind a band at 1024 cm^{-1} which is hidden by the former one in the spectrum recorded in

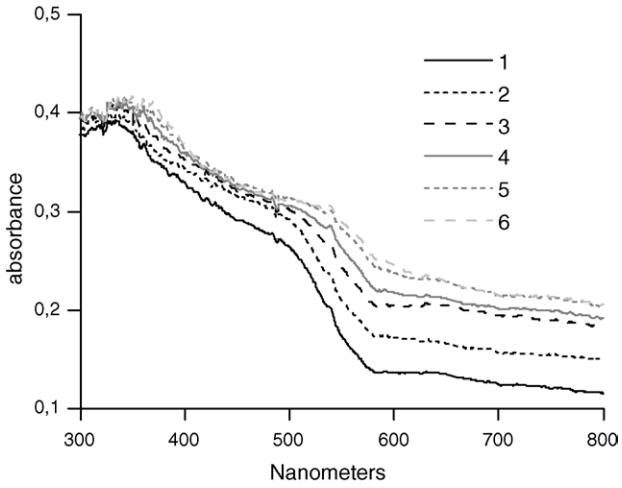

Fig. 4. . UV–vis spectra recorded in parallel to the Raman and EPR spectra in Figs. 2 and 3: at 20 °C after pre-treatment in air at 450 °C (1), at 20 °C after 30 min treatment in a flow of 8.3% O_2, 8.3% C_3H_8/N_2 (24 ml/min) (2) and after stepwise heating with a 10 min isothermal hold at 100, 200, 300 and 400 °C (3–6).

air flow (Fig. 2, spectrum 2). In the corresponding EPR spectrum (Fig. 3, spectrum 2), the original VO^{2+} signal seen also in spectrum 1 (species ***a*** in Table 1) increases in intensity and a new one appears with a slightly higher value for $A_{\|}$ (species ***b*** in Table 1). The spin Hamiltonian parameters $g_{\|}$ and $A_{\|}$ derived by spectra simulation (Table 1) for species ***a*** and ***b*** are characteristic of square–pyramidal VO^{2+} species observed, too, in another supported V–TiO_2 catalyst based on a sulfate-containing anatase carrier [28]. These signals of isolated VO^{2+} species are superimposed by a broad isotropic line arising from magnetically interacting VO^{2+} species (Table 1, Fig. 3). In the respective UV–vis spectrum (Fig. 4, spectrum 2), absorbance increases above 500 nm in the typical range of d–d transitions of reduced V^{4+} species.

These changes are, first of all, a clear evidence that isolated, pentavalent VO_x species are reduced in the presence of the reactant gas mixture. They confirm previous observations made during ODP over V/ZrO_2 [16], V/Al_2O_3 and V/SiO_2 by in situ UV–vis–DRS [17,20] at high-temperature. It is surprising that this reduction occurs already at room temperature with the V/TiO_2 catalyst used here. Furthermore, the simultaneous disappearance of the Raman band at 1034 cm^{-1} and increase of two VO^{2+} EPR hyperfine lines show clearly that this Raman signal, at least in V/TiO_2, cannot be exclusively due to tetrahedral $O{=}V^{5+}O_3$ species as claimed by Burcham et al. [20] but reflects, too, at least two different square–pyramidal or octahedral $O{=}V^{5+}O_4$ moieties. This confirms both previous suggestions that the V=O bond behaves more or less as a diatomic vibrator giving rise to frequencies largely independent on the rest of the molecule [20] as well as the assumption of Gao et al. [14] who regarded the VO_x species on anatase as being connected to the support by four oxygen bridges. Based on this consideration, Raman bands around 1030 cm^{-1} most probably comprise both $O{=}V^{5+}O_3$ as well as $O{=}V^{5+}O_4$ species, the particular geometry may vary within certain limits.

3.3. Effect of temperature-dependent feed treatment

Stepwise increase of the reaction temperature leads to deeper reduction as evidenced by rising UV–vis absorbance above 500 nm (Fig. 4). At the same time, not only the two VO^{2+} EPR hyperfine signals gain intensity, but also the broad isotropic singlet which is characteristic of polymeric V^{4+} species (Fig. 3, spectrum 3, Table 1). Simultaneously, the Raman band at 1024 cm^{-1} drops down. This observation together with the respective increase in the intensity of EPR signal of polymeric V^{4+} species (Fig. 3, spectrum 3) suggests that the Raman band at 1024 cm^{-1} might be due to the V=O vibration of polymeric V_xO_y surface species (Fig. 2). This agrees with previous assignments [20,25]. Moreover, it can be seen that the signals of microcrystalline V_2O_5 decrease sharply above 100 °C and remain constant above 250 °C (Figs. 2 and 5). Consequently, the increase of UV–vis absorbance in the range of V^{4+}/V^{3+} d–d transitions levels off above 250 °C (Fig. 4).

Interestingly, also the Raman bands of the anatase support loose intensity suggesting that not only vanadium-containing species but also TiO_2 is partly reduced. This is readily evident from Fig. 5 in which the relative area of the Raman bands (related to the band area at 20 °C) at 995 (V_2O_5) and 402 cm^{-1} (TiO_2) is plotted as a function of temperature under flowing ODP feed and flowing air, respectively. When the vanadium-free anatase support is treated in the ODP feed mixture, the TiO_2 bands decrease, too, although less pronounced than in the V/TiO_2 catalyst (Fig. 5). To make sure that the observed changes in the Raman spectra are not just caused by temperature-induced modification of the band shape, the catalyst was heated in air flow only. From a comparison of the respective band areas in Fig. 5, the significance of both TiO_2 and V_2O_5 reduction is clearly seen.

An additional evidence for the reduction of TiO_2 is available from low-temperature EPR measurements of the bare anatase support treated in a flow of 8.3% C_3H_8, 8.3% O_2/N_2 for 30 min at 300 and 500 °C, respectively. Well visible EPR signals for Ti^{3+} and O_2^- are detected at −196 °C the intensity of which is highest after pre-treatment at 500 °C (Fig. 6). Their formation can be explained by reduction of Ti^{4+} to Ti^{3+} and electron transfer to an O_2 molecule adsorbing on a Ti^{3+} site. Such

Table 1
Spin Hamiltonian parameters derived from calculated EPR spectra of 6% V/TiO_2 at different stages of the temperature-dependent operando EPR/UV–vis/Raman experiment (Fig. 3, dashed lines, feed composition: 8.3% C_3H_8, 8.3% O_2/N_2)

Spectrum	V species	$g_{\|}$	$g_{\perp}$	$A_{\|}/G$	$A_{\perp}/G$	I_{rel}
20 °C, feed	***a***	1.939	1.973	180.1	54.3	1
	b	1.925	1.983	199.2	76.4	0.4
	c	1.982		–		3.8
250 °C, feed	***a***	1.940	1.973	176.3	55.6	1
	b	1.925	1.983	199.2	77.2	1.2
	c	1.964				9.5
20 °C, feed at end of experiment	***a***	1.933	1.968	175.8	54.6	1
	c	1.959		–		5.2

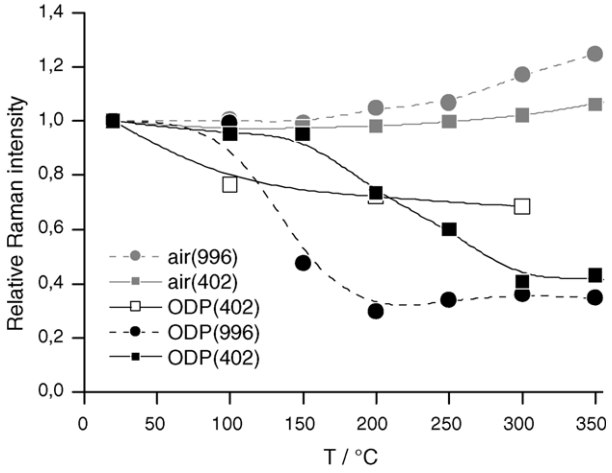

Fig. 5. Relative areas of the Raman bands at 402 cm^{-1} (from anatase) and at 996 cm^{-1} (from V_2O_5) during treatment in air flow (solid grey symbols) and in a flow of 8.3% O_2, 8.3% C_3H_8/N_2 (24 ml/min) (solid black symbols). Open squares reflect the 402 cm^{-1} band of pure anatase in 8.3% O_2, 8.3% C_3H_8/N_2. Band areas at elevated temperature are normalized on the one at 20 °C.

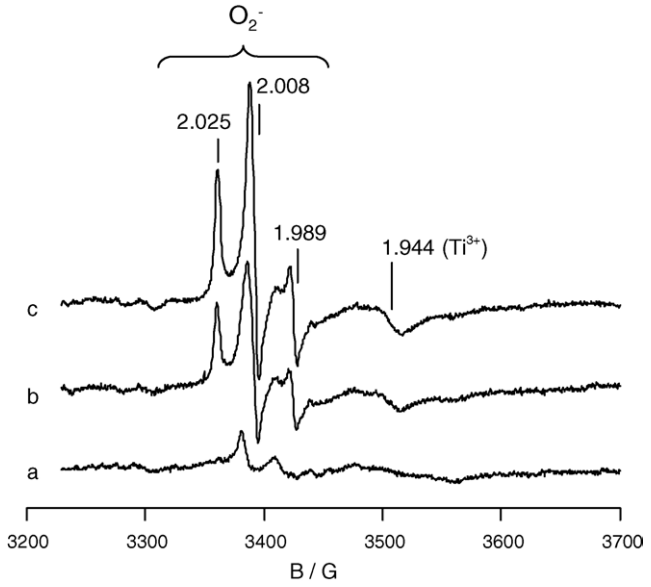

Fig. 6. EPR spectra measured at −196 °C of the bare TiO_2 support after pre-treatment in air flow at 450 °C (a), after 30 min treatment in a flow of 8.3% O_2, 8.3% C_3H_8/N_2 at 300 °C (b) and 500 °C (c), respectively.

electrophilic O_2^- species are often regarded as unselective and as sources for total oxidation [29]. Their presence in the V/TiO_2 catalyst could be a reason for the rather low propene selectivities of less than 15% observed in this work (Fig. 7). In contrast, propene selectivities of more than 60% or 90% (at $X_{propane} \approx 20\%$), respectively, were measured over mesoporous V/SiO_2 and V/Al_2O_3 catalysts, in which no O_2^- species have been detected, during similar operando EPR/UV–vis ODP studies [17].

The more pronounced reduction of TiO_2 in the V-loaded catalyst (Fig. 5) suggests, that the redox activity of the support might be enhanced by the presence of vanadia species dispersed on its surface. Such a phenomenon has already been observed for supported Ag/TiO_2 [30] and points to a strong interaction of TiO_2 and the VO_x species spread on its surface. It has also been

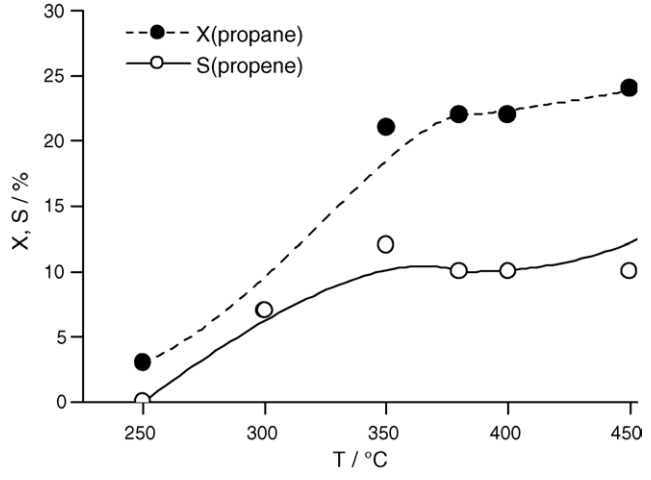

Fig. 7. Propane conversion and propene selectivity measured along with EPR, UV–vis and Raman spectra in Figs. 2–4.

detected by in situ electrical conductivity measurements of V/TiO_2 in comparison to bare TiO_2 in the presence of propane at 400 °C [31]. From this previous study it is clearly evident that the overall electrical conductivity in the presence of propane, which is governed by that of the TiO_2 support, increases stronger for V/TiO_2 in comparison to bare TiO_2. As a reason it was proposed that a spontaneous transfer of electrons proceeds from the Fermi level of vanadia to that of titania [31]. These results are in excellent agreement with the findings presented in this paper.

From Fig. 4 it is evident that the absorbance at higher wavelength, i.e. in the range of d–d transitions of reduced V species, rises with increasing degree of V reduction. In Fig. 8a the difference in absorbance at 800 nm related to the value of the oxidatively pre-treated catalyst at room temperature, Δabs(800 nm), is plotted as a function of temperature during the operando EPR/UV–vis/Raman experiment. To calibrate Δabs(800 nm) with the degree of V reduction, a separate simultaneous TPR/UV–vis experiment was performed, in which Δabs(800 nm) has been followed as a function of the O/V ratio which was calculated from the H_2 consumption (Fig. 8b). From Fig. 8a, a steady-state value of Δabs(800 nm) = 0.093 is obtained. Using the calibration in Fig. 8b, an O/V ratio of 2.43 is obtained for the steady state above 250 °C in Fig. 8a. This corresponds to an average V valence of +4.86. However, it must be taken into account that reduction of TiO_2 could also contribute to the absorbance at 800 nm. Thus, the steady-state V valence of +4.86 represents the lowest possible limit. In any case, this shows clearly, that the majority of the V sites remain pentavalent under reaction conditions, reduction being most probably restricted to the V sites exposed to reactants on the surface. Note that from the TPR/UV–vis experiment only the average V valence can be derived. Even though this is close to +5, it cannot be excluded that some particular V sites are reduced to V^{3+}, as discussed below in relation to the disappearance of one of the two the EPR hyperfine signals.

Further interesting information regarding the behaviour of the different V sites in the V/TiO_2 catalyst under reaction conditions can be obtained from the EPR spectra. From Fig. 3 and Table 1 it can be seen that, besides site ***a***, which is detected under all conditions, a second type of isolated VO^{2+} (site ***b***) is formed as soon as the catalyst comes in contact with the ODP feed. The relative intensity of subspectrum ***b*** passes a maximum around 250 °C and decreases again at higher reaction temperature (not shown). It is not detected anymore in the used catalyst at room temperature after finishing the experiment (Fig. 3, spectrum 4). This suggests, that the corresponding VO^{2+} species is easily reduced to a lower valence state (probably V^{3+}), which is EPR-silent at room temperature due to short relaxation time. In a recent comparative study of VO^{2+} species dispersed on sulfate-containing and sulfate-free anatase, two types of VO^{2+} species with similar spin Hamiltonian parameters as in Table 1 have been observed on the former support and assigned to VO^{2+} directly bound to sulfate (species ***a***) and to TiO_2 (species ***b***) [32]. In contrast, only one type of VO^{2+} species (species ***b***) was detected on

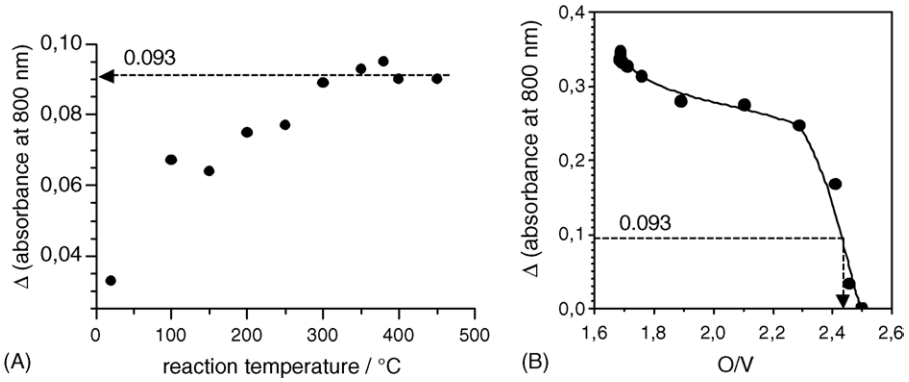

Fig. 8. (a) Difference in absorbance at 800 nm (related to the absorbance of the oxidatively pre-treated catalyst) during heating in 8.3% O_2, 8.3% C_3H_8/N_2 and (b) difference in absorbance at 800 nm (related to the absorbance of the oxidatively pre-treated catalyst) during TPR as a function of the O/V ratio calculated from the H_2 consumption.

sulfate-free anatase. Reduction/reoxidation studies revealed that V species directly bound to sulfate are much faster reoxidized than those connected to TiO_2 only [32]. Thus, it is probable, that the former (species ***a***, Table 1) tend to persist in a higher equilibrium valence state under ODP conditions than the latter (species ***b***, Table 1). With respect to this behaviour, it is likely to assume that the disappearance of species ***b*** with increasing reaction temperature and time on stream might be due to the reduction of VO^{2+} to EPR-silent V^{3+} which is prevented, when VO^{2+} is directly connected to sulfate (species ***a***).

Considering the catalytic parameters, which were acquired simultaneously with the different spectra in Figs. 2–4, it can be seen that propane conversion becomes measurable at 250 °C and increases with temperature until it remains almost constant above 350 °C (Fig. 7). During this time virtually all monomeric and polymeric $O{=}V^{5+}O_x$ surface species and a considerable part of the V_2O_5 crystals are reduced, however, this does not suppress propane conversion. Interestingly, not only propane conversion but also propene selectivity increases with rising temperature. The reason may be due to the reduction of active V surface sites from the pentavalent to the tetravalent state that occurs upon heating in reactant flow. It is well known that the redox potential of V^{5+} is higher than that of V^{4+} suggesting that V^{5+} is a stronger and probably less-selective oxidizing agent than V^{4+}. This agrees well with results found for a variety of other supported VO_x catalysts in the ODP reaction which indicate improved propene selectivities with increasing degree of V site reduction [2,17,33]. In any case, the results in this work clearly show that reduced V species can act as active and selective sites. This is in contrast

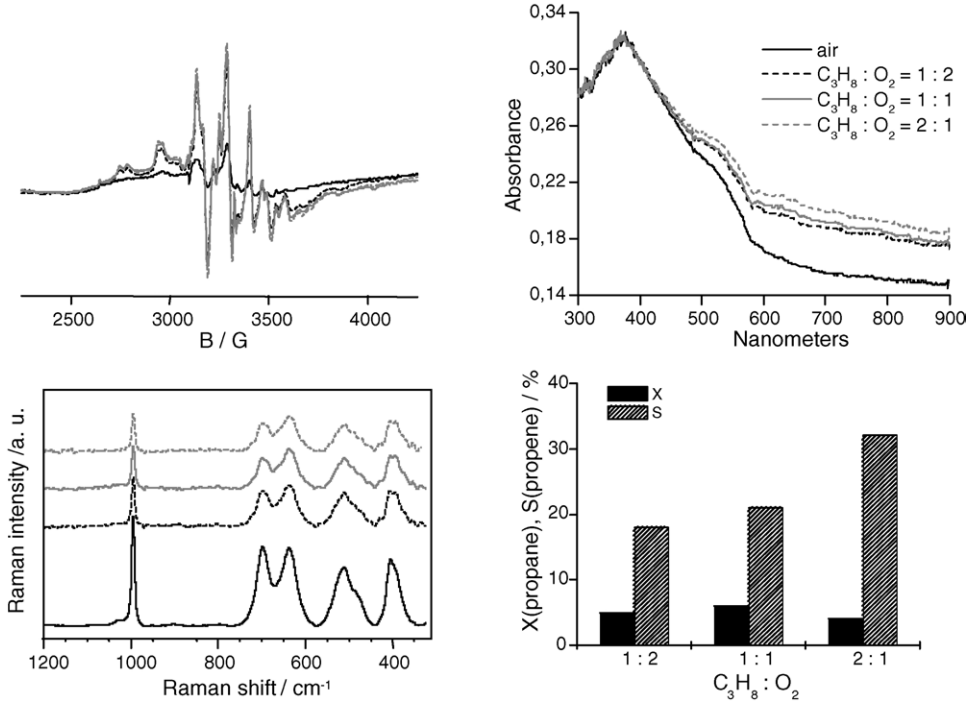

Fig. 9. Operando EPR, UV–vis and Raman spectra as well as propane conversion and propene selectivity measured at 300 °C after 45 min treatment in flows of different C_3H_8: O_2 ratio (N_2 balance 20 ml/min, total flow 24 ml/min).

to observations during ODP over VO_x/ZrO_2 for which it has been claimed that propene selectivity is favoured by pentavalent surface vanadia species and V_2O_5 crystals were ruled out as participants in ODP [16].

3.4. Effect of different C_3H_8: O_2 ratios

For a more detailed study of the relation between V valence and catalytic performance, the C_3H_8/O_2 ratio in the feed was varied while keeping the total flow, the amount of N_2 balance and the temperature at 300 °C constant (Fig. 9). After 1 h in air flow, the C_3H_8/O_2 ratio was kept at 0.5 for 1 h followed by successive 1 h treatments at C_3H_8/O_2 ratios of 1 and 2. The most pronounced change in the spectra is observed upon switching from air flow to a feed containing C_3H_8 and O_2 in a ratio of 0.5. A marked increase of EPR intensity and absorbance in the visible range of the UV–vis spectrum as well as a decrease in Raman band intensity reflect considerable reduction of the catalyst already when oxygen is in excess (Fig. 9). The missing Raman band above 1000 cm^{-1} suggests that both mono- and polymeric VO_x surface species might have been already reduced. The reduction process continues by further lowering the oxygen percentage in the feed, although the changes are much less pronounced in comparison to the one from air to $C_3H_8/O_2 = 0.5$. In the EPR spectra, just the contribution of subsignal *c* increases which is due to interacting VO^{2+} sites while a further loss of Raman band intensity at 995 cm^{-1} reflects ongoing reduction of V_2O_5 crystals.

Interestingly, propane conversion remains roughly unchanged while propene selectivity increases markedly with ongoing reduction of V^{5+} to V^{4+}. This confirms observations from temperature-dependent experiments discussed above and indicates clearly that propene selectivity is favoured by VO^{2+} sites being both highly dispersed on the support surface or part of the outer shell of the V_2O_5 crystals.

4. Conclusions

By comparing the above described results with previous findings having been obtained by single-technique approaches it is readily seen that the triple coupling of operando EPR/UV–vis/Raman spectroscopy provides more authentic information on processes proceeding under reaction conditions and helps to overcome obscurities. Thus, it could be evidenced that isolated $O{=}VO_x$ of varying geometry including square–pyramidal coordination are comprised by the same Raman band around 1034 cm^{-1} although the coordination of these V sites differs. Of the different $V^{5+}O_x$ species, truly isolated ones are most sensitive towards reaction with propane being reduced to VO^{2+} already at room temperature followed by polymeric VO_x surface species and V_2O_5 crystals. Two different types of VO^{2+} species have been detected by EPR from their spin Hamiltonian parameters and, based on previous investigations [32], assigned to VO^{2+} with direct bonding to the sulfate dopant and to TiO_2 only. The latter species is reduced upon time on stream to an EPR-silent valence state (most probably V^{3+}), which might exclude this V species from being an active site.

Despite increasing reduction of V^{5+} to V^{4+} which is clearly evidenced by all three techniques with rising temperature at a constant C_3H_8/O_2 ratio or at constant temperature with rising C_3H_8/O_2 ratio, no deactivation of the catalyst but increasing propene selectivity was observed. In contrast to interpretations based on single-technique approaches [16] this suggests strongly that tetravalent V sites are active and selective.

Furthermore, it has been shown by Raman and EPR spectroscopy that not only vanadia species but also the titania support is reducible under reaction conditions even to a larger extent than in the absence of vanadia species dispersed on its surface. This enhanced redox activity of TiO_2 within the catalyst in comparison to the vanadium-free support (an observation which has been rarely discussed before) might be the reason why turnover frequencies derived for VO_x/TiO_2 in *n*-butane [21] and ethane oxidation [24] are highest in comparison to VO_x supported on other oxides. In the present paper it is shown that isolated VO^{3+} sites, which are only connected by V–O–Ti but not by V–O–V bonds, are reduced first already at room temperature. Since the reduced VO^{2+} species still contain the V=O bond as evidenced by EPR, the reactive oxygen most likely comes from the V–O–Ti bond. This is a strong corroboration that V–O–support units participate in the catalytic cycle as proposed by Banares and Wachs [19], in particular at low V loadings.

Acknowledgements

The authors thank the Federal Ministry for Education and Research of Germany (grant No. 03C3013), the EU (European Funds of Regional Development) and the Federal State of Berlin (Dept. for Science, Research and Culture) for financial support.

References

[1] B.M. Weckhuysen, Chem. Commun. (2002) 97.
[2] M.A. Banares, M.O. Guerriero-Pérez, J.L.G. Fierro, G. Garcia Cortez, J. Mater. Chem. 12 (2002) 3337.
[3] H. Topsøe, J. Catal. 216 (2003) 155.
[4] G. Sankar, J.M. Thomas, C.R.A. Catlow, Top. Catal. 10 (2000) 225.
[5] B.J. Clausen, Catal. Today 10 (1998) 293.
[6] A. Brückner, Chem. Commun. (2001) 2122.
[7] T.A. Nijhuis, S.J. Tinnemans, T. Visser, B.M. Weckhuysen, Phys. Chem. Chem. Phys. 5 (2003) 4361.
[8] J.G. Mesu, A.M.J. van der Erden, F.M.F. de Groot, B.M. Weckhuysen, J. Phys. Chem. B 109 (2005) 3822.
[9] M. Hunger, W. Wang, Chem. Commun. (2004) 548.
[10] F. Thibault-Starzyk, B. Gil, S. Aiello, T. Chevreau, J.P. Gilson, Micropor. Mesopor. Mater. 67 (2004) 107.
[11] A. Brückner, Chem. Commun. (2005) 1761.
[12] A. Brückner, Catal. Rev. Sci. Eng. 45 (2003) 97.
[13] A. Brückner, in: B.M. Weckhuysen (Ed.), In situ Spectroscopy of Catalytic Solids, American Scientific Publishers, Stevenson Ranch, California, 2004 , p. 219 (Chapter 11).
[14] X. Gao, M.A. Banares, I.E. Wachs, J. Catal. 188 (1999) 325.
[15] A. Khodakov, B. Olthof, A.T. Bell, E. Iglesia, J. Catal. 181 (1999) 205.
[16] X. Gao, J.-M. Jehng, I.E. Wachs, J. Catal. 209 (2002) 43.
[17] A. Brückner, Phys. Chem. Chem. Phys. 5 (2003) 4461.
[18] G.T. Wendt, L.-J. Leu, A.T. Bell, J. Catal. 134 (1992) 479.
[19] M.A. Banares, I.E. Wachs, J. Raman Spectrosc. 33 (2002) 359.

[20] L.J. Burcham, G. Deo, X. Gao, I.E. Wachs, Top. Catal. 11/12 (2000) 85.
[21] I.E. Wachs, J.-M. Jehng, G. Deo, B.M. Weckhuysen, V. Guliants, J.B. Benziger, Catal. Today 32 (1996) 47.
[22] G.J. Hutchings, A. Desmartinchomel, R. Olier, J.C. Volta, Nature 368 (1994) 41.
[23] M.A. Bañares, J.H. Cardoso, F. Agulló-Rueda, J.M. Correa-Bueno, J.L.G. Fierro, Catal. Lett. 64 (2000) 191.
[24] M.A. Bañares, M. Martinez-Huerta, X. Gao, I.E. Wachs, J.L.G. Fierro, Stud. Surf. Sci. Catal. 130 (2000) 3125.
[25] G.G. Cortez, M.A. Bañares, J. Catal. 209 (2002) 197.
[26] G.P. Lozos, B.M. Hofman, C.G. Franz, Quantum Chem. Programs Exchange (1973) 265.
[27] G. Centi, S. Perathoner, F. Trifiró, A. Aboukais, C.F. Aissi, M. Guelton, J. Phys. Chem. 96 (1992) 2617.
[28] O.B. Lapina, A.A. Shubin, A.V. Nosov, E. Bosh, J. Spengler, H. Knözinger, J. Phys. Chem. B 103 (1999) 7599.
[29] A. Bielanski, J. Haber, Oxygen in Catalysis, Marcel Dekker Inc., New York, 1991, 43.
[30] W. Grünert, A. Brückner, H. Hofmeister, P. Claus, J. Phys. Chem. B 108 (2004) 5709.
[31] P. Viparelli, P. Ciambelli, J.-C. Volta, J.-M. Herrmann, Appl. Catal. A: Gen. 182 (1999) 165.
[32] A. Brückner, U. Bentrup, J.-B. Stelzer, Z. Anorg. Allg. Chem. (in press).
[33] P. Rybarczyk, H. Berndt, J. Radnik, M.-M. Pohl, O. Buyevskaya, M. Baerns, A. Brückner, J. Catal. 202 (2001) 45.